Advances in Mathematical Sciences and Applications
Vol.18, No.1 (2008), pp.83-104

Gakkōtosho
Tokyo, Japan

NUMERICAL COMPUTATIONS FOR THE SPATIAL SEGREGATION LIMIT OF SOME 2D COMPETITION-DIFFUSION SYSTEMS

Marco Squassina
Dipartimento di Informatica, Università degli Studi di Verona
Cà Vignal 2, Strada Le Grazie 15, I-37134 Verona, Italy
(marco.squassina@univr.it)

Simone Zuccher
Dipartimento di Informatica, Università degli Studi di Verona
Cà Vignal 2, Strada Le Grazie 15, I-37134 Verona, Italy
(zuccher@sci.univr.it)

Abstract. We provide a set of numerical simulations for the spatial segregation limit of two diffusive Lotka-Volterra models in presence of strong competition and inhomogeneous Dirichlet boundary conditions. We consider the classical non-variational quadratic coupling as well as a cubic coupling which makes the problem variational. For both cases we perform a numerical investigation of the limiting density distributions, the front tracking, the segregation rate and the dependence of the shape of the segregated regions upon the size of diffusion coefficients. This approach can be easily extended to the multi-species multi-dimensional case.

Communicated by Editors; Received December 8, 2007.
The first author was partially supported by the MIUR research project "Variational and Topological Methods in the Study of Nonlinear Phenomena".
AMS Subject Classification 35B40, 35K57, 35B35, 92D25

1 Introduction

A interesting problem in the study of population ecology is the understanding, both from a theoretical and numerical point of view, of the strong and competitive interactions between different species. Under suitable assumptions, as the rate ruling the mutual interaction of two different species goes to infinity, competition-diffusion systems usually exhibit a limiting configuration with segregated habitats divided by a smooth interface. We refer the reader to [3–9, 11, 14–18, 20, 21] and in particular to [4, 5, 18] for models involving Dirichlet boundary data and to [6, 11] for those requiring zero-flux boundary conditions. For a complete analysis of the stationary case, we refer to [2]. In the following we will focus the attention on the Dirichlet case, mentioning some of the most recent achievements.

1.1 Recent theoretical results

Let d_u, d_v, λ and κ be all positive constants and consider the following two-species two-dimensional competition-diffusion system

$$\begin{cases} u_t - d_u \Delta u = \lambda u(1-u) - \kappa uv, & \text{in } (0,1)\times(0,1)\times(0,\infty), \\ v_t - d_v \Delta v = \lambda v(1-v) - \kappa uv, & \text{in } (0,1)\times(0,1)\times(0,\infty), \\ u(x,y,t) = \psi(x,y,t), & \text{on } \partial((0,1)\times(0,1))\times[0,\infty), \\ v(x,y,t) = \zeta(x,y,t), & \text{on } \partial((0,1)\times(0,1))\times[0,\infty), \\ u(x,y,0) = u_0(x,y), & \text{in } (0,1)\times(0,1), \\ v(x,y,0) = v_0(x,y), & \text{in } (0,1)\times(0,1). \end{cases} \tag{Q_κ}$$

In [5] Crooks, Dancer, Hilhorst, Mimura and Ninomiya proved that there exists a sequence (u_κ, v_κ) of solutions to (Q_κ) converging, for any $T > 0$, in $L^2((0,1)\times(0,1)\times(0,T))$ as $\kappa \to \infty$ to a bounded segregated state (u_∞, v_∞) such that $w = u_\infty - v_\infty$ solves a limiting free boundary problem (see problem (3.1)), which determines analytically the segregation boundary between the two species in the limit $\kappa \to \infty$. Their study includes the case of time-dependent boundary conditions and possibly different diffusion coefficients. In the same paper the authors perform numerical computations showing the comparison between the contour plots of the solutions of (Q_κ) and those of the free boundary problem, for large values of κ. Quite recently, beside the convergence results on finite-time intervals, in [4], in the case of equal diffusion coefficients $d_u = d_v$ and stationary boundary conditions, Crooks, Dancer and Hilhorst studied the long-term segregation for large interactions, by reducing the system to a single parabolic equation whose solutions have κ-independent uniform bounds. This enables them to use Lyapunov stability arguments to perform the long-term analysis. Indeed, stability often follows from a variational structure yielding an energy functional, bounded and decreasing along the trajectories (see e.g. [10, 23]). Unfortunately, as far as we know, due to the coupling term $-\kappa uv$, system (Q_κ) does not admit a natural Lyapunov functional and a direct analysis is therefore not possible. On

the contrary, system

$$\begin{cases} u_t - d_u\Delta u = \lambda u(1-u) - \kappa u v^2, & \text{in } (0,1)\times(0,1)\times(0,\infty), \\ v_t - d_v\Delta v = \lambda v(1-v) - \kappa v u^2, & \text{in } (0,1)\times(0,1)\times(0,\infty), \\ u(x,y,t) = \psi(x,y,t), & \text{on } \partial((0,1)\times(0,1))\times[0,\infty), \\ v(x,y,t) = \zeta(x,y,t), & \text{on } \partial((0,1)\times(0,1))\times[0,\infty), \\ u(x,y,0) = u_0(x,y), & \text{in } (0,1)\times(0,1), \\ v(x,y,0) = v_0(x,y), & \text{in } (0,1)\times(0,1), \end{cases} \tag{C_κ}$$

admits a Lyapunov energy and, for steady boundary data, a direct study of the spatial segregation phenomena has been recently carried out in [22], where the reader can find references of some physical situation involving such a cubic coupling (e.g. weakly coupled nonlinear Schrödinger system in $\mathbb{R}^3$). Also the Gray-Scott model [13] of reaction-diffusion for chemical species and the Schnackenberg model [19] for an artificial tri-molecular chemical reaction involve a cubic-like coupling. It should be noticed that, in the previously cited works, contrary to the zero flux case, the presence of non-homogeneous boundary conditions is quite hard to manage as the boundary terms which arise when performing integration by parts, in general, cannot be estimated uniformly in κ.

1.2 Goal of the present work

The aim of the paper is to provide a set of meaningful numerical simulations for problems (Q_κ) and (C_κ) for a certain class of segregated initial and boundary conditions, with values between 0 and 1. For both models we investigate the behaviour of the density distributions $u_\kappa(x,y,t)$ and $v_\kappa(x,y,t)$ for large values of t (i.e. in the steady state regime) and κ. As we shall see, (Q_κ) and (C_κ) segregate in a quite different fashion as $-\kappa u_\kappa v_\kappa$ induces a stronger competition compared with the one in (C_κ). Moreover, we provide a numerical strategy to track the interfaces between the segregating boundaries. At this point we need to recall that, while for (Q_κ), at least in the case of equal diffusion coefficients, subtracting the equations of the systems yields a parabolic problem without explicit dependence on the parameter κ (see the bottom of page 657 in [5] and formula (6) in [4]), this is not possible for (C_κ) and for models with more general coupling terms. The method that we propose has the advantage that it can be applied to general situations, without arguing on any limiting problem, but extracting the maxima from the map $\{x \mapsto u_\kappa^2(x,y,t)v_\kappa^2(x,y,t)\}$ at a fixed $y \in [0,1]$ for very large values of t (the steady state regime) and κ. We also provide a comparison, for (Q_κ), on how the interface plots from [5] for the free boundary problem almost perfectly fit the boundary line detected by our method. Another very hard problem to handle analytically is the rate of convergence to zero for the following integral, which measures, in some sense, the segregation rate

$$J_\kappa(t) = \int_0^1 \int_0^1 u_\kappa^2(x,y,t)v_\kappa^2(x,y,t)dxdy. \tag{1.1}$$

This integral is know to vanish at least as κ^{-1}, but it is expected to decade more rapidly, say as $\kappa^{-\sigma}$ for some $\sigma > 1$ (see, e.g., the indication given in the stationary case by [1, (iii)

of Lemma 4.1]). We confirm this fact numerically, and we extrapolate the values of σ for both models by graphical comparison. The above integral arises naturally for (C_κ) by multiplying for u_κ (resp. v_κ) the equation of u_κ (resp. v_κ). For the canonical coupling, system (Q_κ), these multiplications yield different quantities, but we evaluate and plot $J_\kappa(t)$ also in this case, for the comparison with the values for (C_κ) to be meaningful. The afore mentioned analysis is performed for a fixed set of initial-boundary data and for fixed values of λ and d_u, d_v. We also show how the shape of the segregating regions as well as the rates of decay of $J_\kappa(t)$ is influenced by the size of the diffusion coefficients. Finally, we briefly discuss the case where the boundary data are segregated but the initial data are not. Numerical simulations reveal that the crucial assumption is boundary segregation, rather than initial data segregation. We stress that our numerical approach can be easily implemented in the case of three (or more) populations species. To the authors' knowledge, the only other papers in literature which consider numerical methods to study the two-species spatial segregation limit for Lotka-Volterra type models are [5] for Dirichlet boundary conditions and [12] for the Neumann boundary conditions.

2 Discretization and numerical solution

2.1 Numerical method

Systems (Q_κ) and (C_κ) are solved numerically by employing second order, centered, finite differences on a generally uneven grid both in space and time. Let the computational domain be $\Omega \times [0,T] = [0,1] \times [0,1] \times [0,T]$ with $(x,y) \in \Omega$ and $T > 0$. If N_x and N_y denote respectively the number of grid points in x and y, after spatial discretization system (Q_κ) (or system (C_κ)) reads as

$$\begin{cases} \mathbf{u}_t = \mathbf{h}(\mathbf{u}) \\ \mathbf{u}(\Omega, 0) = \mathbf{u}_0, \end{cases} \tag{2.1}$$

where $\mathbf{u}$ and $\mathbf{h}(\mathbf{u})$ are respectively the vector of unknowns and the spatial residual at each grid point (i,j) organized as follows ($\delta = 1$ refers to (Q_κ), $\delta = 2$ to (C_κ))

$$\begin{aligned} \mathbf{u} &= [\dots, u_l, v_l, \dots]^T, \\ \mathbf{h}(\mathbf{u}) &= [\dots, d_u \Delta u_l + \lambda u_l(1-u_l) - \kappa u_l v_l^\delta, d_v \Delta v_l + \lambda v_l(1-v_l) - \kappa u_l^\delta v_l, \dots]^T, \\ &\text{with} \quad l = i + N_x(j-1), \quad i = 1 \dots N_x, \quad j = 1 \dots N_y. \end{aligned} \tag{2.2}$$

It should be noted that $\mathbf{u}_0$ in (2.1) is the initial condition, whereas the boundary conditions, which are assumed to be steady, are already included in the spatial discretization. The second-order, implicit, Crank-Nicolson method is used for time discretization in order to avoid possible numerical-stability problems associated with explicit methods and to allow relatively large time steps. By introducing $\Delta t = t^{n+1} - t^n$, system (2.1) is recast as

$$\begin{cases} \mathbf{u}^{n+1} = \mathbf{u}^n + \dfrac{\Delta t}{2} \left[\mathbf{h}(\mathbf{u}^{n+1}) + \mathbf{h}(\mathbf{u}^n) \right] \\ \mathbf{u}(\Omega, 0) = \mathbf{u}_0, \end{cases} \tag{2.3}$$

which is a nonlinear functional of the unknown vector $\mathbf{u}^{n+1}$. A complete Newton linearization is, thus, performed and the Jacobian is recomputed at each Newton iteration so as to ensure the fast convergence guaranteed by the method. Here the Jacobian is calculated analytically but, alternatively, it could have been computed numerically by employing the definition of derivative. The latter strategy, however, would have been very time consuming. If $\mathbf{u}_r^{n+1}$ denotes the solution corresponding to the r-th Newton iteration at $t = t_{n+1}$, namely at the $(n+1)$-th time step, convergence to $\mathbf{u}^{n+1}$ is considered reached as $||\mathbf{u}_r^{n+1} - \mathbf{u}_{r-1}^{n+1}||_2 < 10^{-12}$. Between three and four Newton iterations were required for the cases here considered. The initial guess for computing $\mathbf{u}^{n+1}$ is $\mathbf{u}^n$. The steady solution for $t \to \infty$ is considered achieved when $||\mathbf{u}^{n+1} - \mathbf{u}^n||_2 < \epsilon$, where ϵ is the tolerance chosen by the user. Results presented in this work were typically obtained with $\epsilon = 10^{-4}$ or smaller. System (2.3) has some band structure but is clearly very sparse due to the use of finite differences in two dimensions (i.e. the number of nonzero elements of the matrix of dimension m is $\mathcal{O}(m)$ instead of $\mathcal{O}(m^2)$, with $m = 2N_xN_y$ in our case). Therefore, we used the matrix CSR (Compressed Storage Row) format, which requires one double array and one integer array of length equal to the number of non-zero elements, and one integer array of length equal to the dimension of the system. Being the LU decomposition not affordable in such conditions, we preferred to use a semi-iterative solver for (nonsymmetric) sparse matrices, namely the BiCGStab (BiConiugate Gradient Stabilized [24]) method preconditioned by ILU(0) (Incomplete LU factorization with no fill-in), already tailored to CSR format. Although the discretization allows uneven x- and y-grid and variable Δt, results are shown for $N_x = N_y = 120$ ($\Delta x = \Delta y \approx 8.265 \cdot 10^{-3}$) and $\Delta t = 2.5 \cdot 10^{-4}$.

2.2 Initial-boundary conditions

As we use the same set of segregated initial-boundary conditions throughout the paper, we introduce their analytical expression, followed by some figures in the next pages. Analogous linear density distributions on the boundary have been considered also in [5, Section 4]. Assuming $\alpha \in (0, 1/2]$ and $\beta \in [0, 1]$, the (steady) boundary conditions for $u(x, y, t)$ and $v(x, y, t)$ are, for any $t \geq 0$, defined as follows:

$$\psi(x,0,t) = \begin{cases} \beta - \dfrac{\beta}{\alpha}x, & \text{if} \quad 0 \leq x < \alpha, \\ 0, & \text{if} \quad \alpha \leq x \leq 1, \end{cases}$$

$$\psi(x,1,t) = \begin{cases} \beta - \dfrac{\beta}{1-\alpha}x, & \text{if} \quad 0 \leq x < 1-\alpha, \\ 0, & \text{if} \quad 1-\alpha \leq x \leq 1, \end{cases}$$

$$\psi(0,y,t) = \beta,$$

$$\psi(1,y,t) = 0,$$

and

$$\zeta(x,0,t) = \begin{cases} 0, & \text{if} \quad 0 \le x < \alpha, \\ -\dfrac{\alpha\beta}{1-\alpha} + \dfrac{\beta}{1-\alpha}x, & \text{if} \quad \alpha \le x \le 1, \end{cases}$$

$$\zeta(x,1,t) = \begin{cases} 0, & \text{if} \quad 0 \le x < 1-\alpha, \\ \dfrac{\beta(\alpha-1)}{\alpha} + \dfrac{\beta}{\alpha}x, & \text{if} \quad 1-\alpha \le x \le 1, \end{cases}$$

$$\zeta(0,y,t) = 0,$$

$$\zeta(1,y,t) = \beta.$$

Initial conditions $u(x,y,0)$ and $v(x,y,0)$ used in the numerical simulations are obtained by linearly interpolating the boundary conditions for every $(x,y) \in [0,1] \times [0,1]$, so as to ensure their segregation. More explicitly, for any $\alpha \neq 1/2$, we set:

$$u_0(x,y) = \begin{cases} 0, & \text{if} \quad 0 \le y \le \dfrac{x-\alpha}{1-2\alpha}, \\ \beta\left(1 - \dfrac{x}{y(1-2\alpha)+\alpha}\right), & \text{if} \quad \dfrac{x-\alpha}{1-2\alpha} < y \le 1, \end{cases}$$

$$v_0(x,y) = \begin{cases} \dfrac{x-(y(1-2\alpha)+\alpha)}{1-(y(1-2\alpha)+\alpha)}\beta, & \text{if} \quad 0 \le y \le \dfrac{x-\alpha}{1-2\alpha}, \\ 0, & \text{if} \quad \dfrac{x-\alpha}{1-2\alpha} < y \le 1. \end{cases} \tag{2.4}$$

The particular case $\alpha = 1/2$ reduces the initial conditions to:

$$u_0(x,y) = \begin{cases} \beta\,(1-2x)\,, & \text{if} \quad 0 \le x \le \dfrac{1}{2}, \\ 0, & \text{if} \quad \dfrac{1}{2} < x \le 1, \end{cases}$$

$$v_0(x,y) = \begin{cases} 0, & \text{if} \quad 0 \le x \le \dfrac{1}{2}, \\ \beta(2x-1), & \text{if} \quad \dfrac{1}{2} \le x \le 1. \end{cases} \tag{2.5}$$

The initial conditions $u_0(x,y)$ and $v_0(x,y)$ are reported in figure 1 for $\alpha = 0.2$ and $\beta = 0.5$ (u on the left, v on the right). From the figure and from the analytical expressions (2.4) and (2.5) it is clear that the initial conditions satisfy the boundary constrains. The two dimensional maps of $u_0(x,y)$ and $v_0(x,y)$ (with $\alpha = 0.2$ and $\beta = 0.5$) are reported in figure 2 in order to visually emphasize the spatial segregation. As we will see (cf. Section 7), the crucial assumption for the spatial segregation to occur is the boundary segregation rather than the initial data segregation.

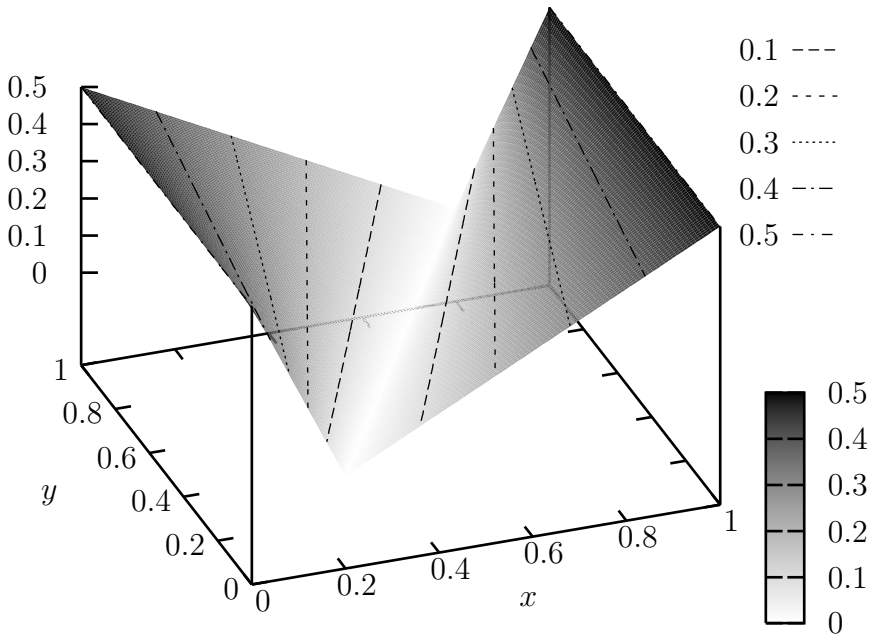

Figure 1: Segregated initial conditions $u_0(x,y)$ and $v_0(x,y)$. Here $\alpha = 0.2$ and $\beta = 0.5$ (u appears on the left, v on the right).

3 Density distributions

The main goal of [4, 5, 18, 22] is to provide an analytical justification for the spatial segregation phenomena of (Q_κ) and (C_κ) on finite-time intervals or in the long term. More precisely, considering for instance the initial-boundary conditions introduced in the previous section, we recall from [5, Section 3], for model (Q_κ), the following

Theorem 3.1. *Let $T > 0$. Then there exists a diverging sequence (κ_m) and $u_\infty, v_\infty \in L^\infty$ with*

$$(u_{\kappa_m}, v_{\kappa_m}) \to (u_\infty, v_\infty) \quad \text{in } L^2((0,1)\times(0,1)\times(0,T)) \times L^2((0,1)\times(0,1)\times(0,T)),$$

as $m \to \infty$, where $0 \le u_\infty, v_\infty \le 1$ and $u_\infty v_\infty = 0$ in $(0,1)\times(0,1)$. Moreover, $w = u_\infty - v_\infty$ is the unique weak solution to the free boundary problem

$$\begin{cases} w_t - \Delta D(w) = \lambda w(1-|w|), & \text{in } (0,1)\times(0,1)\times(0,\infty), \\ Dw(x,y,t) = d_u\psi(x,y,t) - d_v\zeta(x,y,t), & \text{on } \partial((0,1)\times(0,1))\times[0,\infty), \\ w(x,y,0) = u_0(x,y) - v_0(x,y), & \text{in } (0,1)\times(0,1), \end{cases} \tag{3.1}$$

where

$$D(\sigma) = \begin{cases} d_u\sigma, & \text{if } \sigma \ge 0, \\ d_v\sigma, & \text{if } \sigma < 0. \end{cases}$$

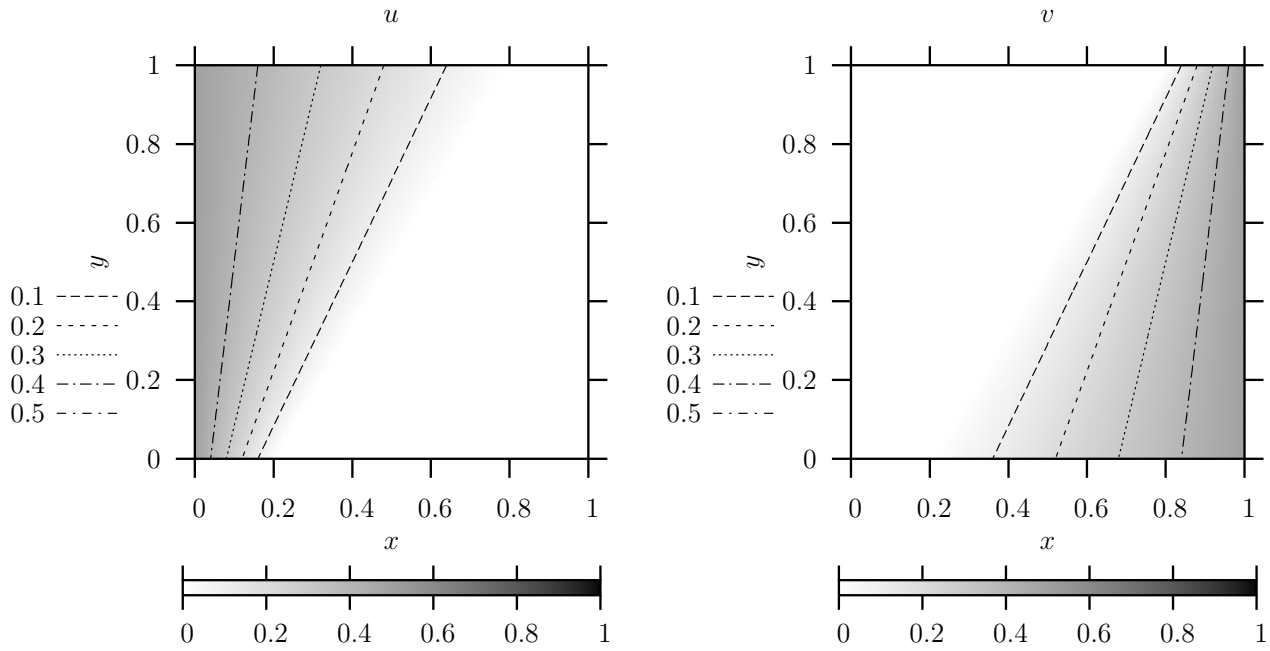

Figure 2: 2D map and contour plot of the segregated initial conditions $u_0(x, y)$ and $v_0(x, y)$. Here $\alpha = 0.2$ and $\beta = 0.5$.

In [22], with our choice of initial-boundary data, for model (C_κ) it was proved the following

Theorem 3.2. *There exist two diverging sequences* $(\kappa_m), (t_m)$ *and* $u_\infty, v_\infty \in H^1 \cap L^\infty$ *with*

$$(u_{\kappa_m}(t_m), v_{\kappa_m}(t_m)) \to (u_\infty, v_\infty) \quad \text{in } L^p((0,1)\times(0,1)) \times L^p((0,1)\times(0,1)) \text{ for any } p \geq 2,$$

as $m \to \infty$, *where* $0 \leq u_\infty, v_\infty \leq 1$ *and* $u_\infty v_\infty = 0$ *in* $(0,1)\times(0,1)$. *Moreover*

$$-d_u \Delta u_\infty \leq \lambda u_\infty (1 - u_\infty), \quad -d_v \Delta v_\infty \leq \lambda v_\infty (1 - v_\infty),$$

and $u_\infty|_{\partial(0,1)^2} = \psi$, $v_\infty|_{\partial(0,1)^2} = \zeta$.

As we have already pointed out in the introduction, due to the cubic coupling, in the case of (C_κ), it seems not possible to derive a free boundary problem analogous to the one appearing in the statement of Theorem 3.1. Thus, we were naturally led to perform some numerical computations of the limiting density distributions $u(x, y)$ and $v(x, y)$ for (C_κ) as $t, \kappa \to \infty$ and to compare the results with those for (Q_κ). For the test shown hereafter different values of κ were used with $\alpha = 0.2$, $\beta = 0.5$, $d_u = 1.5$, $d_v = 1.0$, $\lambda = 50$. Figures referring to model (Q_κ) are presented first because they allow a direct comparison with those from [5] (available for $\kappa = 10^2, 10^3, 10^4$), which can be used for the numerical validation of our code. Figure 3 shows the contour plot superimposed to the 2D map of the steady state solutions $u(x, y)$ and $v(x, y)$ obtained with $\kappa = 10^4$ for model (Q_κ). By comparing this figure with the last figure on page 650 of [5] one can notice a very good qualitative agreement. In order to appreciate more quantitatively

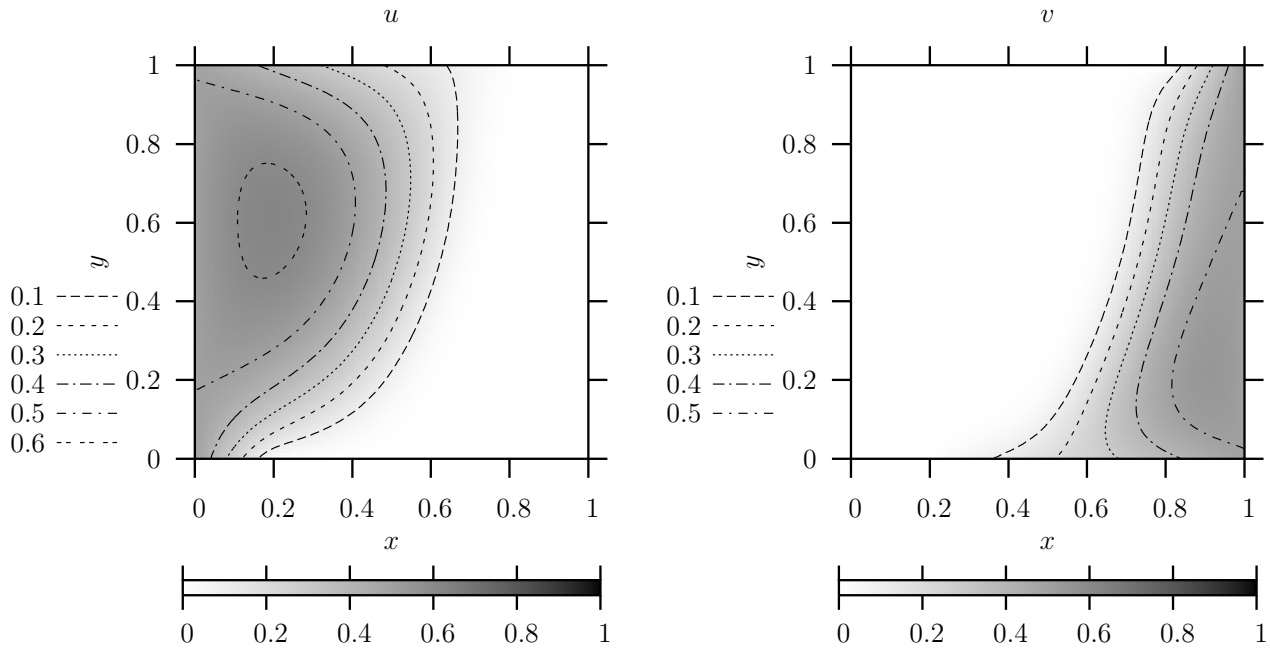

Figure 3: Model (Q_κ), $\kappa = 10^4$, 2D map and contour plot of the steady state solution $u(x, y)$ and $v(x, y)$. Here $\alpha = 0.2$, $\beta = 0.5$, $d_u = 1.5$, $d_v = 1.0$, $\lambda = 50$.

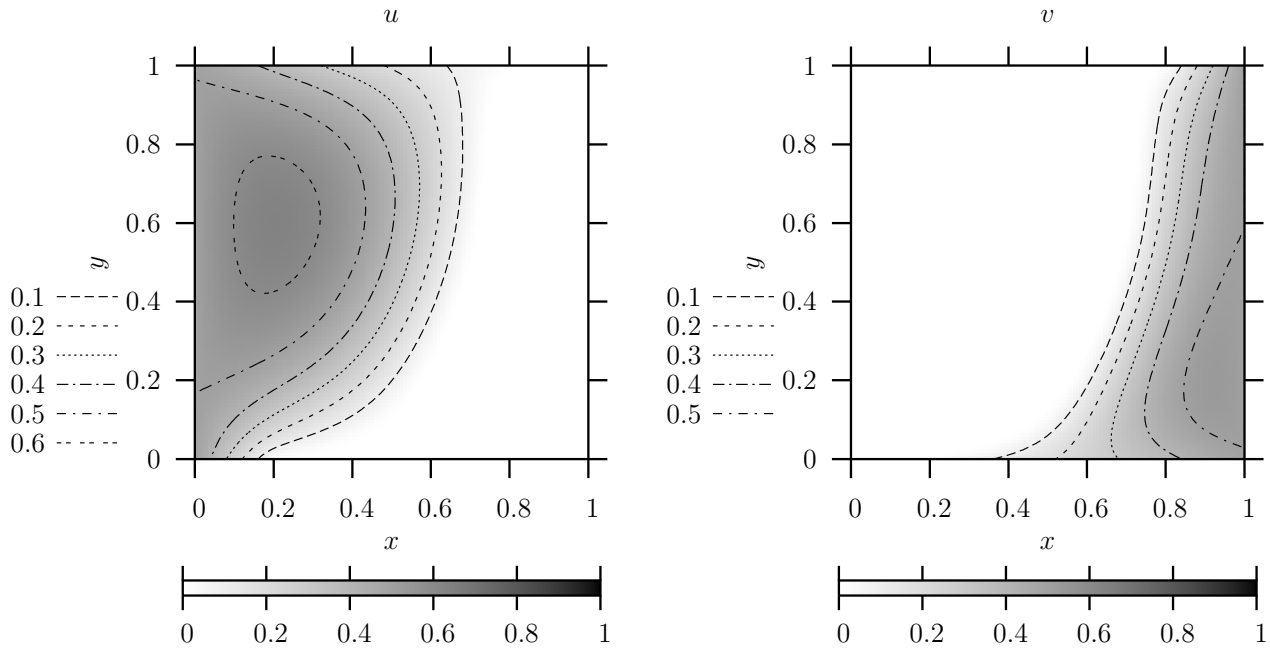

Figure 4: Model (Q_κ), $\kappa = 10^6$, 2D map and contour plot of the steady state solution $u(x, y)$ and $v(x, y)$. Here $\alpha = 0.2$, $\beta = 0.5$, $d_u = 1.5$, $d_v = 1.0$, $\lambda = 50$.

the overlapping with [5], cross sections of $u(x, y)$ and $v(x, y)$ at $y = 1/3$ are reported in figure 5. The solid line (present result, $\kappa = 10^4$) and the empty circles (results by [5],

$\kappa = 10^4$) match quite remarkably, thus confirming the reliability of the numerical code developed for these experiments. The main interest is in the limit $\kappa \to \infty$, for which

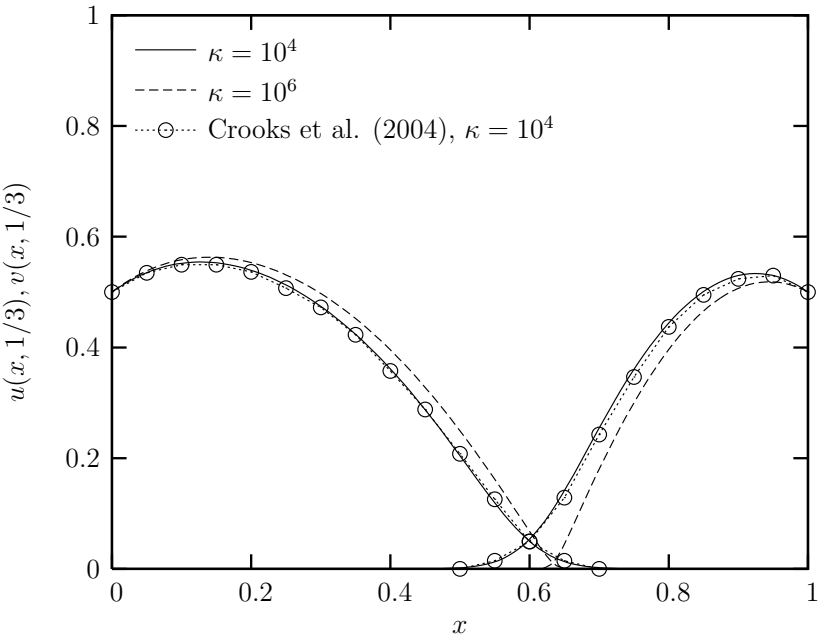

Figure 5: Model (Q_κ), cross sections of the steady state solution $u(x,y)$ and $v(x,y)$ at $y = 1/3$. Comparison with [5] for $\kappa = 10^4$ and between $\kappa = 10^4$ and $\kappa = 10^6$. Here $\alpha = 0.2$, $\beta = 0.5$, $d_u = 1.5$, $d_v = 1.0$, $\lambda = 50$.

the models predicts the spatial segregation of the species. Hence, by looking at the cross sections, one would expect to see the intersection between the two curves $u(x,1/3)$ and $v(x,1/3)$ moving downwards for increasing κ. This is confirmed by the results obtained for $\kappa = 10^6$. The 2D maps (figure 4) might look quite similar to the case $\kappa = 10^4$, but the quantitative comparison between the cross sections at $y = 1/3$ (figure 5) shows that for larger values of κ the intersection between the two curves occurs where both u and v are very close to zero. As a consequence, the segregation front can be more precisely identified at the location $\bar{x}$ where this occurs ($\bar{x} = 0.633$). Model (C_κ) was investigated by employing the same coefficients $\alpha, \beta, d_u, d_v, \lambda$ as well as the same initial conditions used for model (Q_κ) so as to allow a direct comparison. The 2D maps of u and v (figure 6) indicate a quite different scenario with respect to the one found for the quadratic model. Even if the diffusivity of u is 50% larger than the one of v, the region occupied by the v-species is visibly wider. This can be interpreted, at least from a qualitative point of view, by observing that the first equation of system (C_κ) can be viewed as system (Q_κ) with a smaller (location-dependent) competition coefficient, $\kappa_v = \kappa v < \kappa$ for the first equation and $\kappa_u = \kappa u < \kappa$ for the second equation. Of course, this is based on the fact that $[0,1] \times [0,1]$ is an invariant region for both systems. Figure 6 shows that the segregated state is not reached yet (for $\kappa = 10^4$) since there still are overlapping regions where both u and v coexist. By increasing κ to 10^6 (figure 7), the segregating regions of

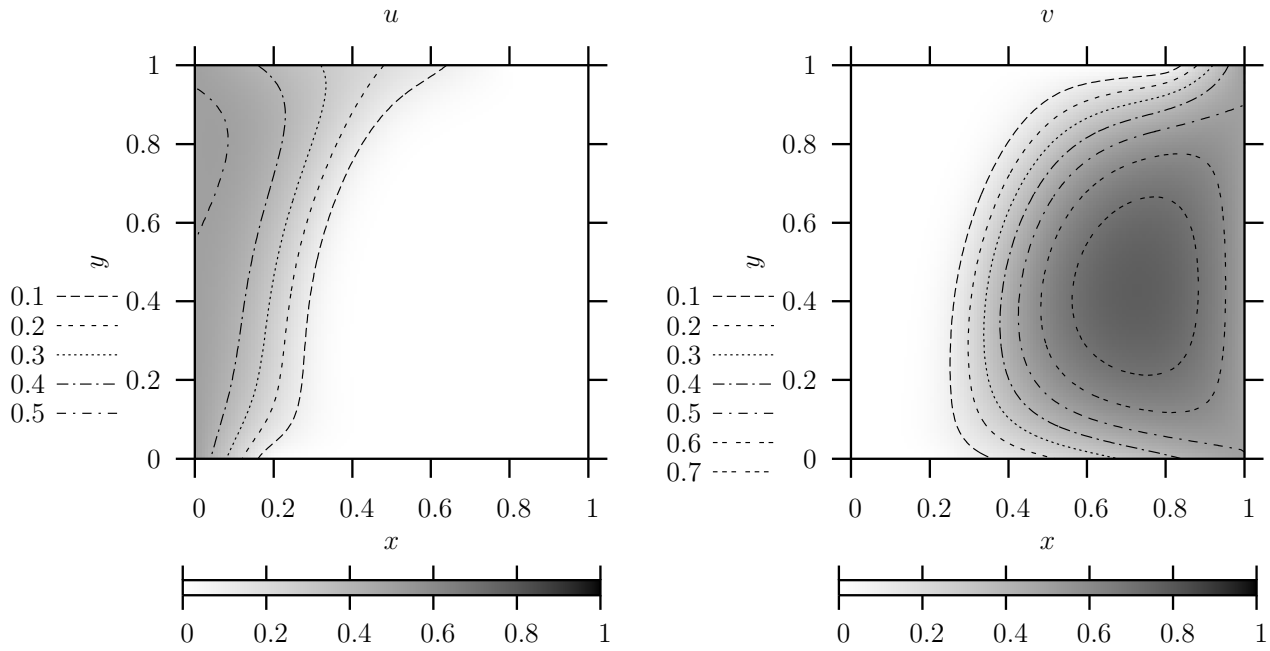

Figure 6: Model (C_κ), $\kappa = 10^4$, 2D map and contour plot of the steady state solution $u(x, y)$ and $v(x, y)$. Here $\alpha = 0.2$, $\beta = 0.5$, $d_u = 1.5$, $d_v = 1.0$, $\lambda = 50$.

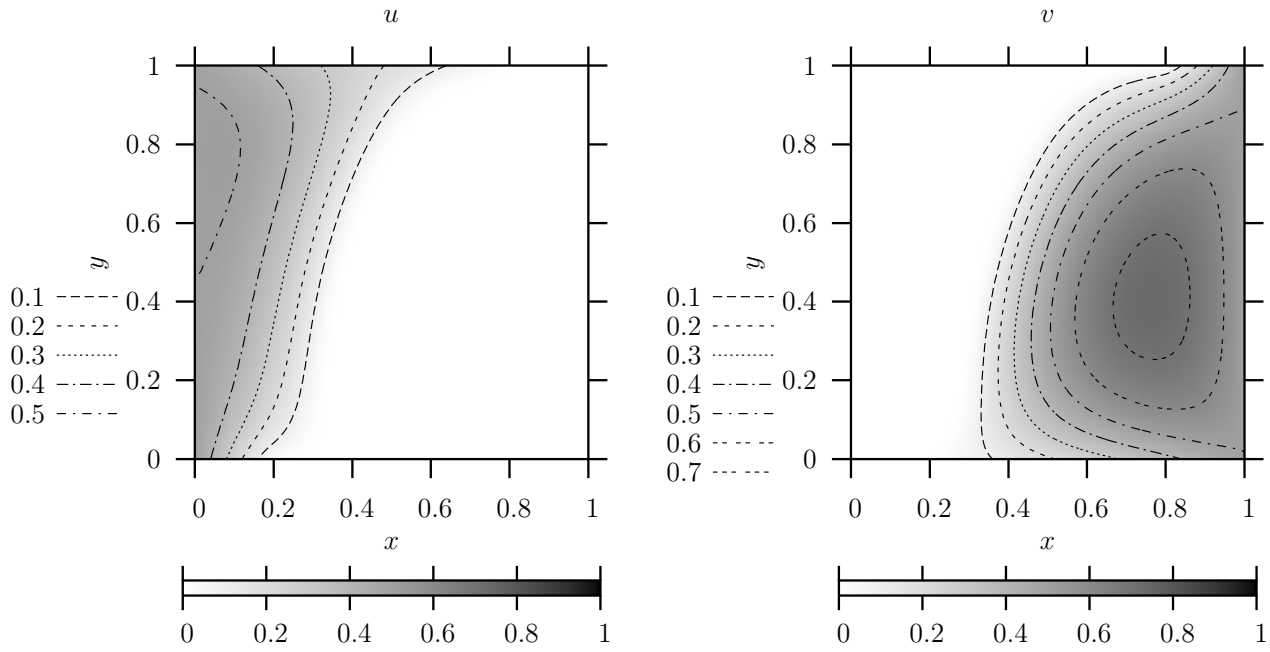

Figure 7: Model (C_κ), $\kappa = 10^6$, 2D map and contour plot of the steady state solution $u(x, y)$ and $v(x, y)$. Here $\alpha = 0.2$, $\beta = 0.5$, $d_u = 1.5$, $d_v = 1.0$, $\lambda = 50$.

u and v become clearer. Figure 8 reports the cross sections of the steady-state solution $u(x, y)$ and $v(x, y)$ at $y = 1/3$. It is quite evident that, also for system (C_κ), segregation

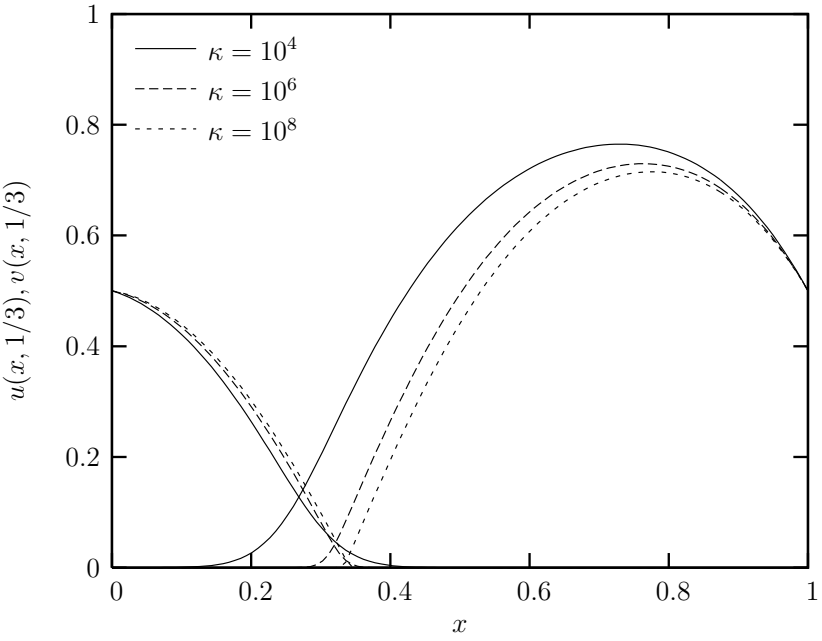

Figure 8: Model (C_κ), cross sections of the steady state solution $u(x,y)$ and $v(x,y)$ at $y = 1/3$, comparison between $\kappa = 10^4$, $\kappa = 10^6$ and $\kappa = 10^8$. Here $\alpha = 0.2$, $\beta = 0.5$, $d_u = 1.5$, $d_v = 1.0$, $\lambda = 50$.

is reached in the limit $\kappa \to \infty$.

4 Front tracking

The problem of tracking the separation front between the segregating regions occupied by u and v for κ and t very large is nontrivial [4, 5, 12]. It has to be stressed again that, while for model (Q_κ) the segregating boundary can be analytically represented (cf. [5]) by the free boundary problem (3.1), this does not seem possible for (C_κ) . Here we propose a very simple way of front-tracking the boundaries in the case of two species which are segregated in two regions divided by a single line connecting a point on the lower border $\{y = 0\}$ to the corresponding point on the upper border $\{y = 1\}$ of the square. For more complex cases (e.g. three species populations or two species segregated in different areas surrounded by a closed lines, etc.) this idea can be extended without much complication.

In the segregating regime, the function $\varphi := u^2v^2$ tends to vanish. As seen for the cross sections reported in the previous paragraph (see figures 5 and 8), φ achieves its maximum (at fixed y) where the cross sections intersect. As κ goes to infinity, $\bar{x}$ (i.e. the x-spatial location at y fixed corresponding to the intersection between u and v) is a good estimate of the front between the two species. In other words, if γ stands for the limiting front

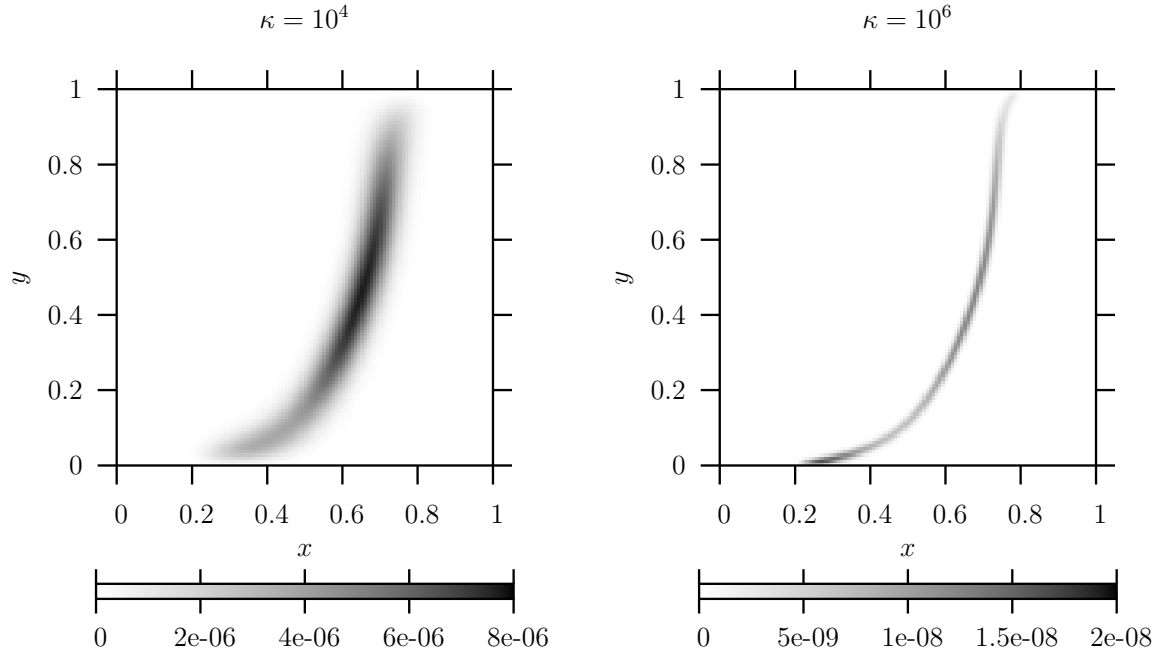

Figure 9: Model (Q_κ), 2D map of φ, comparison between the solutions for $\kappa = 10^4$ and $\kappa = 10^6$. Here $\alpha = 0.2$, $\beta = 0.5$, $d_u = 1.5$, $d_v = 1.0$, $\lambda = 50$.

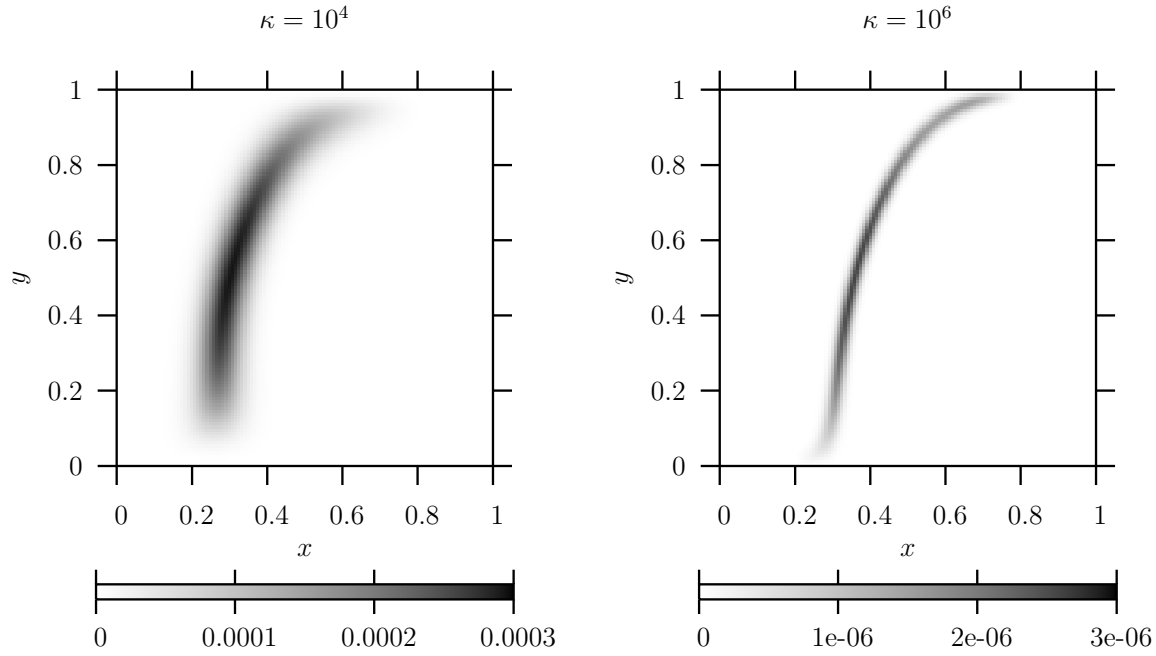

Figure 10: Model (C_κ), 2D map of φ, comparison between the solutions for $\kappa = 10^4$ and $\kappa = 10^6$. Here $\alpha = 0.2$, $\beta = 0.5$, $d_u = 1.5$, $d_v = 1.0$, $\lambda = 50$.

curve, it can be parametrized as

$$y \mapsto \gamma(y), \qquad \varphi(\gamma(y), y) := \max_{\xi \in [0,1]} \varphi(\xi, y).$$

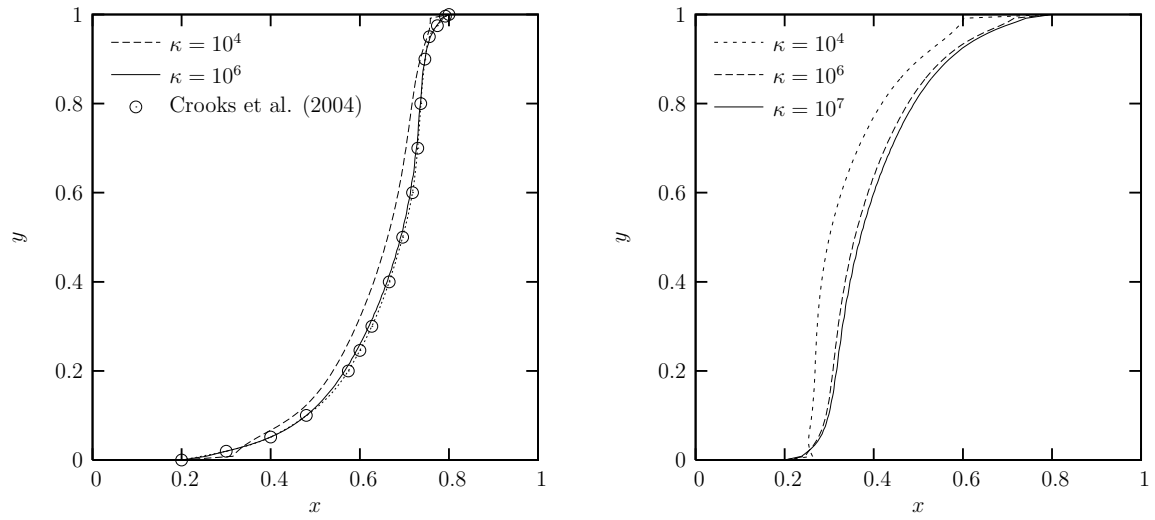

Figure 11: Front tracking of the interface between u and v for different values of κ, comparison between model (Q_κ) and (C_κ). Here $\alpha = 0.2$, $\beta = 0.5$, $d_u = 1.5$, $d_v = 1.0$, $\lambda = 50$.

Figure 9 shows a comparison between 2D maps of φ obtained with $\kappa = 10^4$ and $\kappa = 10^6$ for model (Q_κ). Visually, one can clearly see that for $\kappa \to \infty$ the region where φ is nonzero becomes very narrow so that the front can be extracted simply by arguing as indicated above. The very same remarks hold true for model (C_κ), reported in figure 10. Here it is interesting to note that $\kappa = 10^6$ is still not sufficient to state that the species are completely segregated. In fact, φ is not as small as for model (Q_κ), but this was expected by looking at figure 8. Figure 11 reports the interfaces between the species obtained by connecting the locations of the maxima of φ. The solid line of the figure on the left compares extremely well with results from [5] obtained by employing, instead, numerical computation of the free boundary problem (3.1). For model (C_κ), as seen before, the limit $\kappa \to \infty$ can be considered reached for κ not less than 10^7 (for $\kappa > 10^7$ the front in figure 8 remains essentially unchanged).

5 Segregation rate

In the investigation of spatial segregation phenomena, the analytical determination of an explicit convergence rate of the solutions towards the limiting state is a very difficult task. In fact, to the authors' knowledge, only in [2, Theorem 2], for the stationary two-species Lotka-Volterra system, an explicit convergence rate, i.e. $\kappa^{-1/6}$, is obtained. The key point in getting this result is, once again, to reduce the system to a single equation (if $d_u = d_v$, subtracting the two equations yields an harmonic function), which is successful only for (Q_κ) due to equal competition coupling terms. Hence, it seems natural to retrive some information on the segregation rate. An object which plays this role and arises in a natural way in (C_κ) from the standard multiplication of the equation of u_κ by u_κ (or

of the equation of v_κ by v_κ) is the integral J_κ. Here J_κ is the value of integral $J_\kappa(t)$ in (1.1) for large t and κ (namely in the steady state regime $u_\kappa(t) \approx u$ and $v_\kappa(t) \approx v$). Figure 12 shows the comparison between the values of J_κ computed, for the two models,

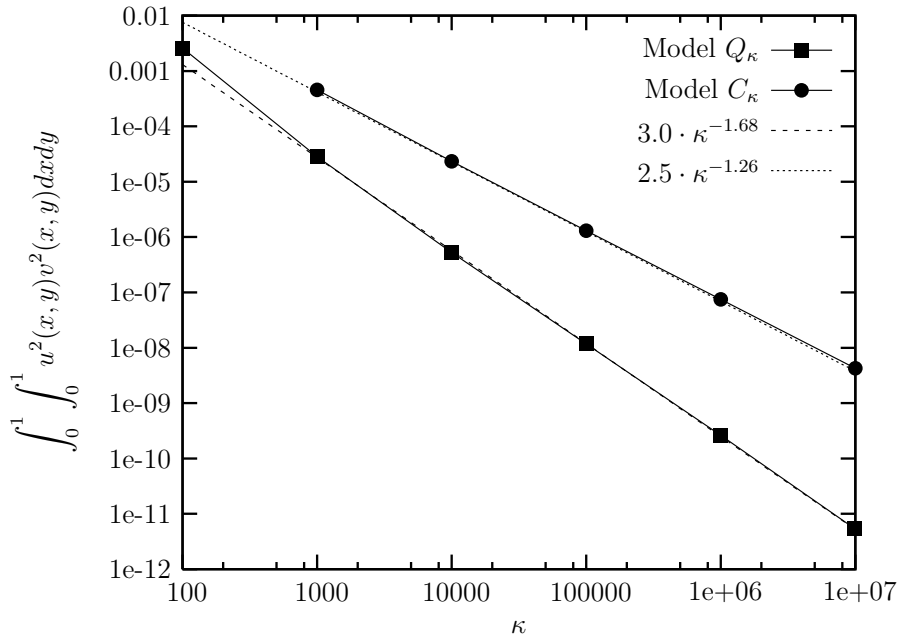

Figure 12: Segregation rate J_κ as a function of κ for models (Q_κ) and (C_κ). Here $\alpha = 0.2$, $\beta = 0.5$, $d_u = 1.5$, $d_v = 1.0$, $\lambda = 50$.

as a function of κ. As predicted in [22] for (C_κ), it must be, at least

$$\sup_{\kappa \geq 1} \kappa J_\kappa < \infty.$$

For (Q_κ), a variant of this was proved in [5, Lemma 2.3], namely, for any $T > 0$,

$$\sup_{\kappa \geq 1} \kappa \int_0^T \int_0^1 \int_0^1 u_\kappa v_\kappa \eta dx dy dt < \infty,$$

where $\eta = \eta(x, y) > 0$ is the first eigenfunction of the Laplace operator $-\Delta$ with homogeneous boundary conditions. We originally suspected that the decay rated of J_κ as $\kappa \to \infty$ could be stronger than κ^{-1} for both models (cf., in the stationary case, [1, (iii) of Lemma 4.1]) and different between the two models. In fact, the numerical experiments that we performed show that J_κ decays as $3.0 \cdot \kappa^{-1.68}$ for model (Q_κ) and as $2.5 \cdot \kappa^{-1.26}$ for model (C_κ). The different decay rates can be easily justified by recalling again that system (C_κ) can be seen as system (Q_κ) with a smaller competition coefficient $\kappa_u = \kappa v < \kappa$ for the first equation and $\kappa_v = \kappa u < \kappa$ for the second equation.

6 Dependence on diffusion coefficients

In this section we consider the dependence of the shape of the segregated regions and of the decay rate of J_κ upon the diffusion parameters d_u and d_v. For model (Q_κ) the decay

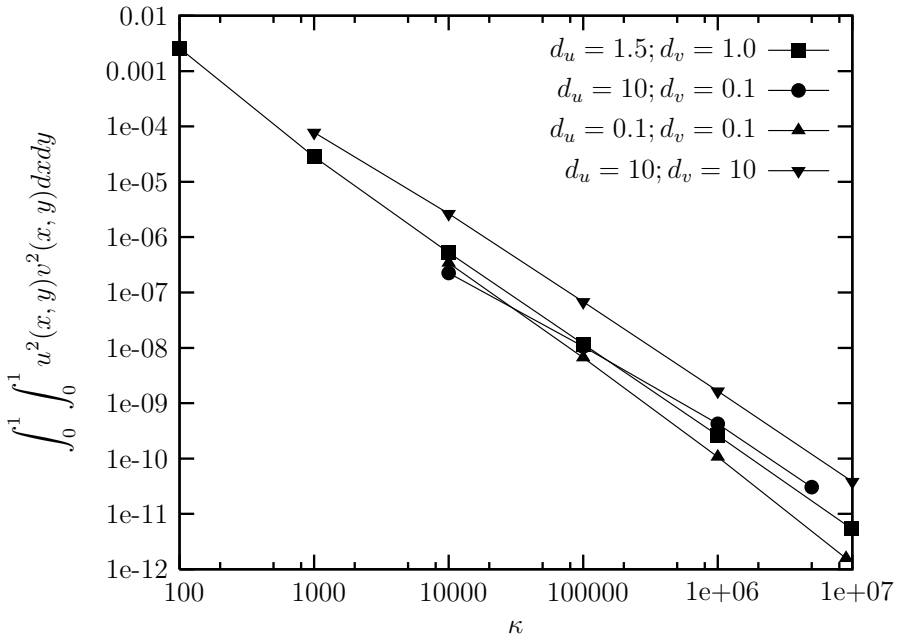

Figure 13: Segregation rate J_κ for model (Q_κ) as a function of κ. Here $\alpha = 0.2$, $\beta = 0.5$, $\lambda = 50$.

of J_κ occurs more or less at the same rate as long as d_u and d_v are the same or at least on the same order of magnitude (figure 13), whereas the line connecting the calculated points is less straight for $d_u = 10$ and $d_v = 0.1$, namely when the ratio between the diffusion coefficients is far from 1. The 2D maps look as expected (see figure 14), with the most diffusive species u ($d_u = 10$ and $d_v = 0.1$) occupying almost the whole available territory when segregation is reached. When the diffusion is the same for both species (figure 15), results are symmetric (as the boundary conditions), but different solutions are obtained depending on how large the diffusion is with respect to the other parameters involved. For instance, when the diffusion is small (figure 15 on the right) both species reach large densities, while their density remains small if the diffusion is large (figure 15 on the left). Figure 16, referred to model (C_κ), confirms a behavior similar to figure 13 except for the difference in the decay rate of J_κ. A remarkable difference between the models tested is found for the density distribution of the species when one is much more diffusive than the other one, as reported in figure 17 for model (C_κ) and $d_u = 10$, $d_v = 0.1$ (this figure should be compared with figure 14). Clearly, species u features a behavior quite similar to what was found for the case $d_u = d_v = 10$ for model (Q_κ), while species v resembles the behavior found for the case $d_u = d_v = 0.1$ for model (Q_κ).

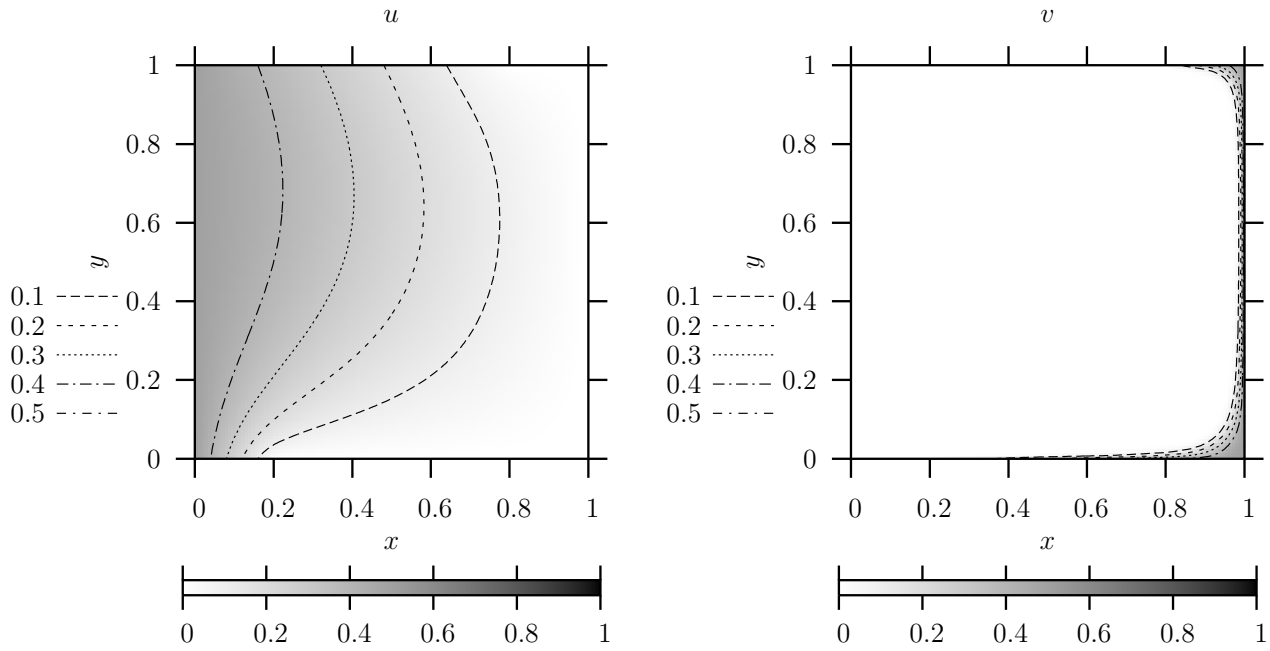

Figure 14: Model (Q_κ), $\kappa = 10^6$, 2D map and contour plot of the steady state solution $u(x, y)$ and $v(x, y)$. Here $\alpha = 0.2$, $\beta = 0.5$, $d_u = 10$, $d_v = 0.1$, $\lambda = 50$.

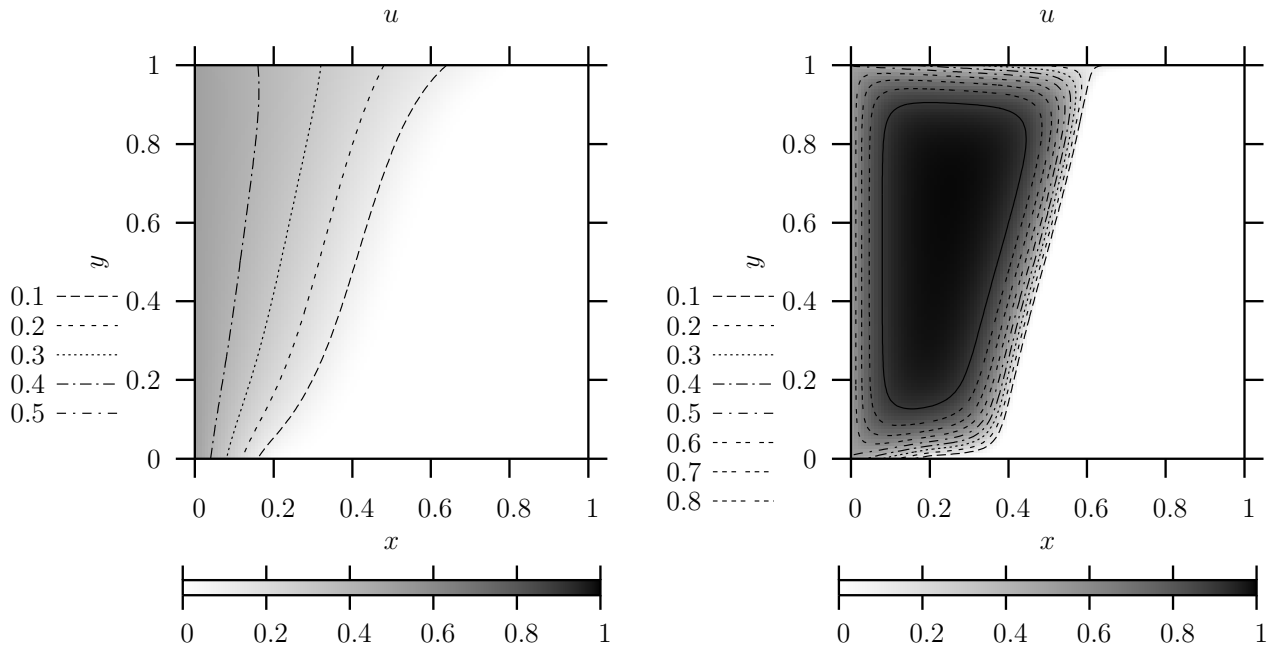

$d_u = d_v = 10$ $\qquad$ $d_u = d_v = 0.1$

Figure 15: Model (Q_κ), $\kappa = 10^6$, 2D map and contour plot of the steady state solution $u(x, y)$ for different values of the diffusivity coefficients. Here $\alpha = 0.2$, $\beta = 0.5$, $\lambda = 50$.

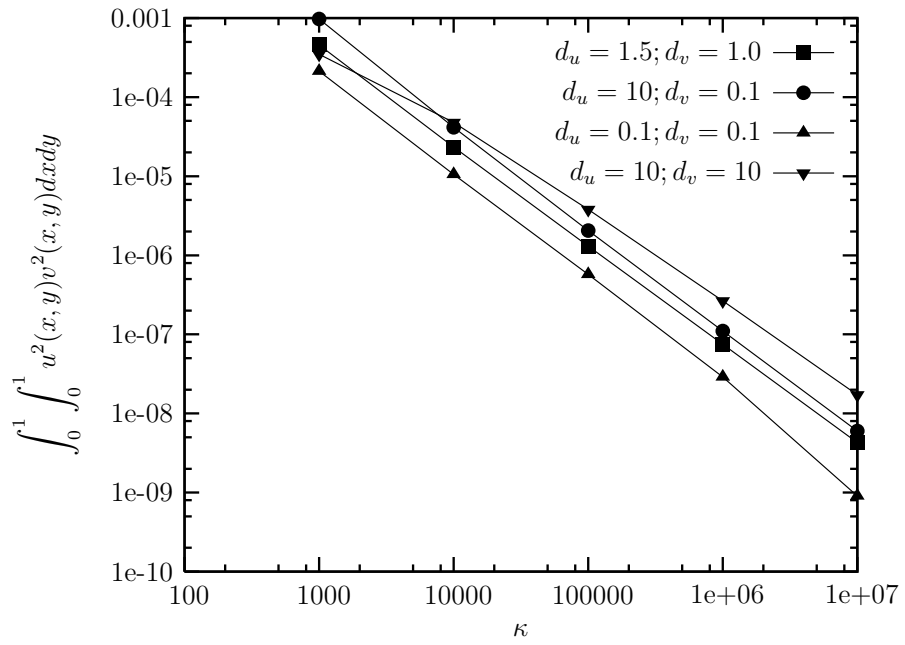

Figure 16: Segregation rate J_κ for model (C_κ) as a function of κ. Here $\alpha = 0.2$, $\beta = 0.5$, $\lambda = 50$.

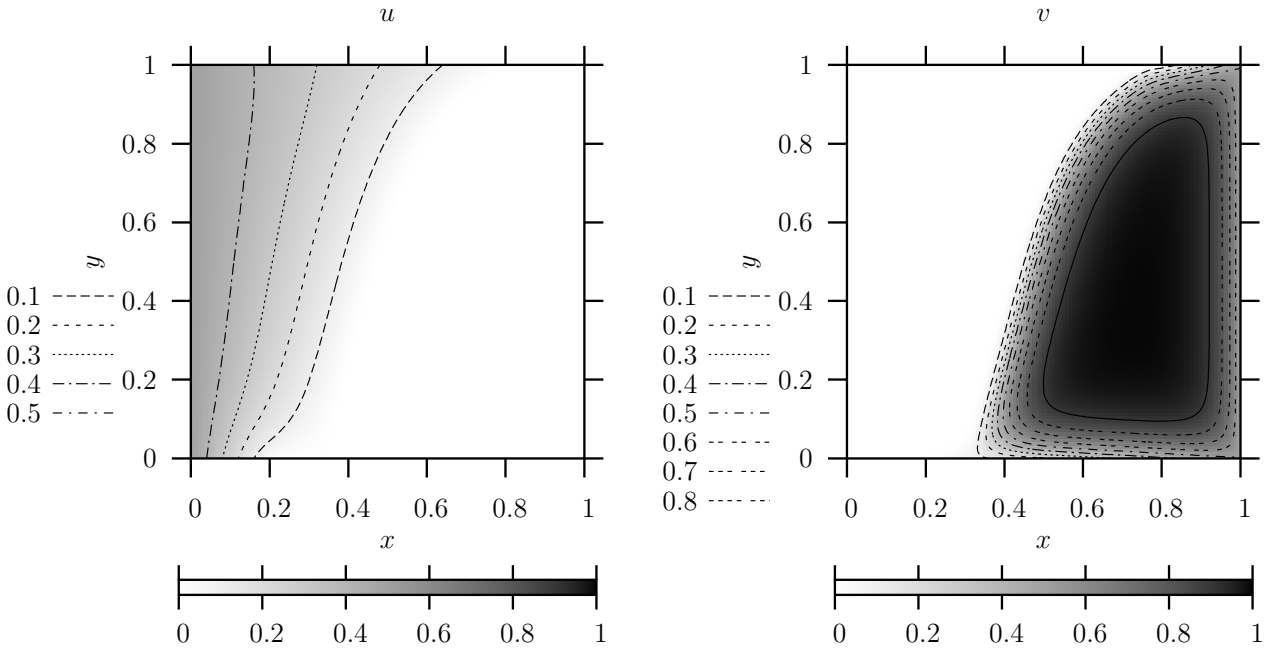

Figure 17: Model (C_κ), $\kappa = 10^6$, 2D map and contour plot of the steady state solution $u(x, y)$ and $v(x, y)$. Here $\alpha = 0.2$, $\beta = 0.5$, $d_u = 10$, $d_v = 0.1$, $\lambda = 50$.

7 Non-segregated initial data

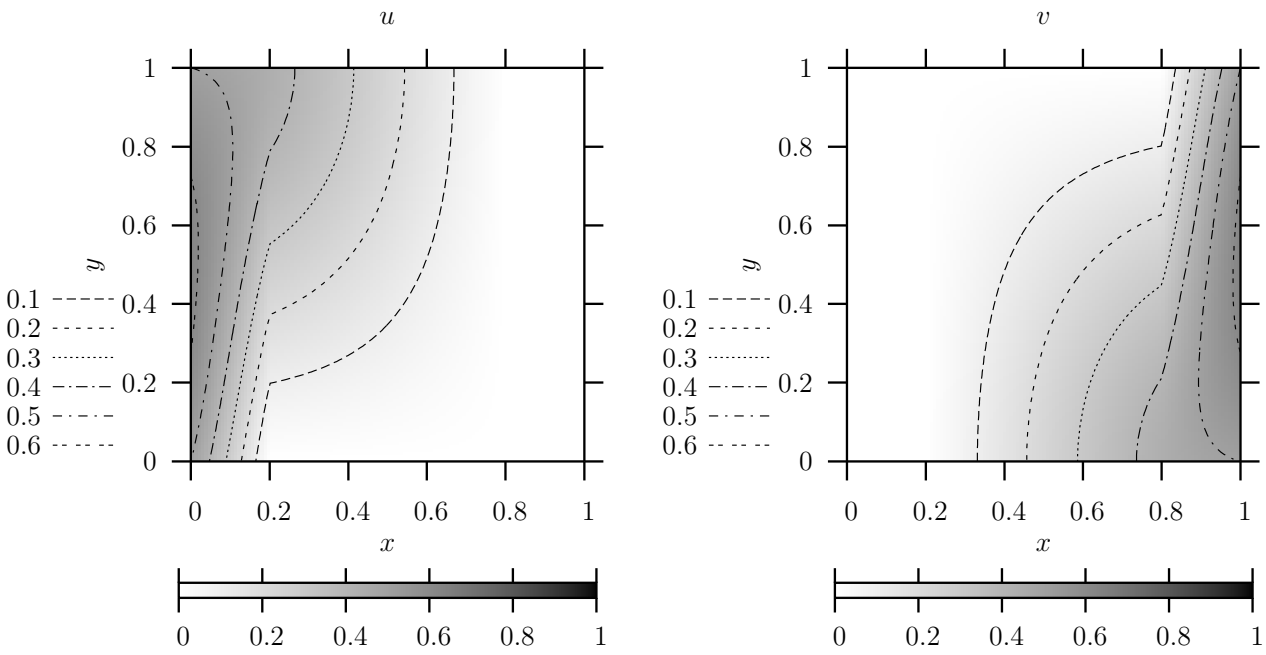

Figure 18: 2D map and contour plot of the non-segregated initial conditions $u_0(x, y)$ and $v_0(x, y)$. Here $\alpha = 0.2$ and $\beta = 0.5$ for the boundary.

Contrary to the case of (Q_κ), model (C_κ) admits a natural Lyapunov functional Λ_κ, that can be used to study, in the case of steady boundary data, the long-term behaviour of the solutions (cf. [22]). By reducing to the case of homogeneous boundary conditions, taking $\tilde{u}_\kappa = u_\kappa - U$, $\tilde{v}_\kappa = v_\kappa - V$ (here $U(x, y)$ and $V(x, y)$ denote the harmonic extensions of the boundary data ψ and ζ), the energy functional Λ_κ can be written as

$$\Lambda_\kappa(t) = \frac{1}{2}\int_0^1\int_0^1 |\nabla \tilde{u}_\kappa(t)|^2 + \frac{1}{2}\int_0^1\int_0^1 |\nabla \tilde{v}_\kappa(t)|^2 - \lambda\int_0^1\int_0^1 \frac{u_\kappa^2(t)}{2} - \frac{u_\kappa^3(t)}{3}$$
$$- \lambda\int_0^1\int_0^1 \frac{v_\kappa^2(t)}{2} - \frac{v_\kappa^3(t)}{3} + \frac{\kappa}{2}\int_0^1\int_0^1 u_\kappa^2(t)v_\kappa^2(t).$$

In particular, as Λ_κ is non-increasing on $[0, \infty)$ (cf. [22, Theorem 2.10]), it is possible to check that there exist three positive constants A, B, C such that

$$A \le \Lambda_\kappa(t) \le B + C\kappa\int_0^1\int_0^1 u_0^2 v_0^2, \qquad t \ge 0.$$

Hence, aiming to get κ-uniform a priori estimates for u_κ and v_κ in H^1, a natural assumption to bound $\Lambda_\kappa(t)$ uniformly in κ and in time is that $u_0 v_0 = 0$, namely segregated initial data (also in [5], the numerical experiments were carried out under this assumption). However, tests starting with non-segregated initial conditions (still remaining segregated

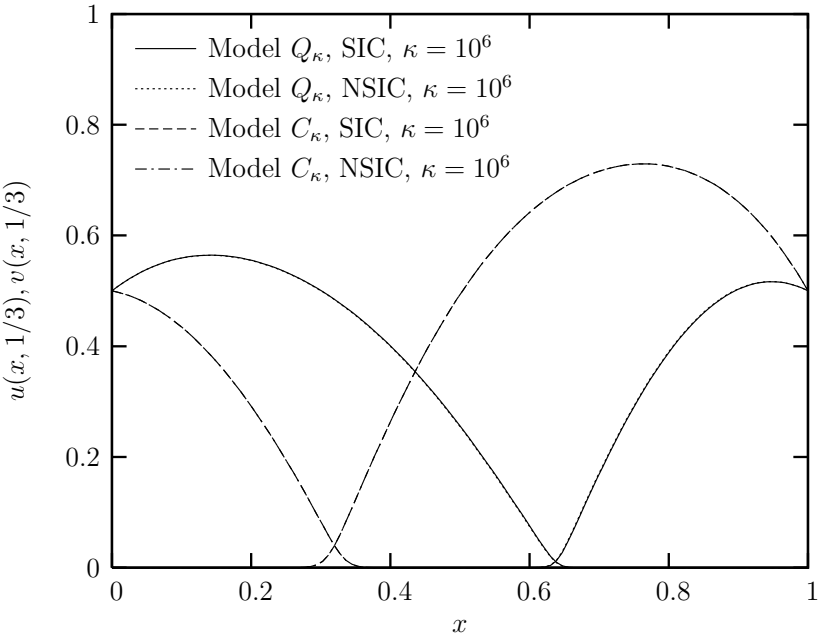

Figure 19: Cross sections of the steady state solution $u(x, y)$ and $v(x, y)$ at $y = 1/3$, for model (C_κ) and (Q_κ) obtained from segregated initial conditions or non-segregated ones. Here $\alpha = 0.2$ and $\beta = 0.5$, $d_u = 1.5$, $d_v = 1.0$, $\lambda = 50$.

along the boundary) reveal that this assumption is not crucial for the species isolation to appear. The initial conditions we consider are obtained by linearly interpolating the boundary conditions, at fixed x, between their values on the border $\{y = 0\}$ and the border $\{y = 1\}$. The linearly interpolated values were further multiplied by the factor $(-x^2 + x + 1)(-y^2 + y + 1)$ so as to amplify the solution in the neighbourhood of the square center and, thus, enhance mixing between the species. Figure 18 reports the 2D map and contour plot of the non-segregated initial conditions employed. For a quantitative comparison, cross sections for the two models are shown in figure 19. In conclusion, no dependence on the initial condition is found.

8 Concluding remarks

Numerical experiments focused on various aspects of the spatial segregation phenomena in two-species two-dimensional competition-diffusion systems with large interactions have been considered. The analysis was motivated by some recent theoretical results on models (Q_κ) and (C_κ). In the case of (C_κ) a limiting free boundary problem for predicting the front of the segregating regions cannot be explicitly obtained. Consequently, we implemented a numerical procedure to compute the front line by employing the maxima of u^2v^2 for $\kappa, t \to \infty$. The rate of spatial segregation as well as the dependence of the shape of the segregated regions upon the diffusion parameters have been investigated. In

particular, we confirmed that the segregation occurs with a rate faster than κ^{-1}, fact that could be conjectured in light of some previous analytical results. Finally, we observed that initial-data segregation has no influence on the final shape of the segregated regions.

References

[1] M. Conti, S. Terracini, and G. Verzini. Nehari's problem and competing species systems. *Ann. Inst. H. Poincaré Anal. Non Linéaire*, 19(6):871–888, 2002.

[2] M. Conti, S. Terracini, and G. Verzini. Asymptotic estimates for the spatial segregation of competitive systems. *Adv. Math.*, 195(2):524–560, 2005.

[3] E.C.M. Crooks, E.N. Dancer, and D. Hilhorst. Fast reaction limit and long time behavior for a competition-diffusion system with dirichlet boundary conditions. *Discrete Contin. Dyn. Syst. B*, 8:39–44, 2007.

[4] E.C.M. Crooks, E.N. Dancer, and D. Hilhorst. On long-time dynamics for competition-diffusion systems with inhomogeneous dirichlet boundary conditions. *Topol. Meth, Nonlinear Anal.*, 30:1–36, 2007.

[5] E.C.M. Crooks, E.N. Dancer, D. Hilhorst, M. Mimura, and H. Ninomiya. Spatial segregation limit of a competition-diffusion system with Dirichlet boundary conditions. *Nonlinear Anal. Real World Appl.*, 5(4):645–665, 2004.

[6] E.N. Dancer and Z. Zhang. Dynamics of Lotka-Volterra competition systems with large interaction. *J. Differential Equations*, 182(2):470–489, 2002.

[7] N. Dancer. Competing species systems with diffusion and large interactions. *Rend. Sem. Mat. Fis. Milano*, 65:23–33 (1997), 1995.

[8] S-I. Ei, R. Ikota, and M. Mimura. Segregating partition problem in competition-diffusion systems. *Interfaces Free Bound.*, 1(1):57–80, 1999.

[9] S.-I. Ei and E. Yanagida. Dynamics of interfaces in competition-diffusion systems. *SIAM J. Appl. Math.*, 54(5):1355–1373, 1994.

[10] A. Haraux. *Systèmes dynamiques dissipatifs et applications*, volume 17 of *Recherches en Mathématiques Appliquées*. Masson, Paris, 1991.

[11] D. Hilhorst, M. Iida, M. Mimura, and H. Ninomiya. A competition-diffusion system approximation to the classical two-phase Stefan problem. *Japan J. Indust. Appl. Math.*, 18(2):161–180, 2001.

[12] R. Ikota, M. Mimura, and T. Nakaki. Numerical computation for some competition-diffusion systems on a parallel computer. *12th International Conference on Domain Decomposition Methods*, 2001.

[13] K.J. Lee, W.D. McCormick, Qi Ouyang, and H.L. Swinney. Pattern formation by interacting chemical fronts. *Science*, 261(5118):192–194, 1993.

[14] H. Matano and M. Mimura. Pattern formation in competition-diffusion systems in nonconvex domains. *Publ. Res. Inst. Math. Sci.*, 19(3):1049–1079, 1983.

[15] J. Mawhin. The legacy of Pierre-François Verhulst and Vito Volterra in population dynamics. In *The first 60 years of nonlinear analysis of Jean Mawhin*, pages 147–160. World Sci. Publ., River Edge, NJ, 2004.

[16] M. Mimura. Spatial distribution of competing species. In *Mathematical ecology (Trieste, 1982)*, volume 54 of *Lecture Notes Biomath.*, pages 492–501. Springer, Berlin, 1984.

[17] M. Mimura and K. Kawasaki. Spatial segregation in competitive interaction-diffusion equations. *J. Math. Biol.*, 9(1):49–64, 1980.

[18] T. Namba and M. Mimura. Spatial distribution of competing populations. *J. Theoret. Biol.*, 87(4):795–814, 1980.

[19] J. Schnackenberg. Simple chemical reaction systems with limit cycle behaviour. *J. Theoret. Biol.*, 81:389–400, 1979.

[20] N. Shigesada, K. Kawasaki, and E. Teramoto. Spatial segregation of interacting species. *J. Theoret. Biol.*, 79(1):83–99, 1979.

[21] N. Shigesada, K. Kawasaki, and E. Teramoto. The effects of interference competition on stability, structure and invasion of a multispecies system. *J. Math. Biol.*, 21(2):97–113, 1984.

[22] M. Squassina. On the long term spatial segregation for a competition-diffusion system. *Asymptotic Anal.*, 57:83–103, 2008.

[23] R. Temam. *Infinite-dimensional dynamical systems in mechanics and physics*, volume 68 of *Applied Mathematical Sciences*. Springer-Verlag, New York, second edition, 1997.

[24] H.A. van der Vorst. Bi-CGSTAB: a fast and smoothly converging variant of Bi-CG for the solution of nonsymmetric linear systems. *SIAM J. Sci. Statist. Comput.*, 13(2):631–644, 1992.